Antitumor Activity, X-ray Crystal Structure, and DNA Binding Properties of Thiocoraline A, a Natural Bisintercalating Thiodepsipeptide

Ana Negri,[†] Esther Marco,[†] Verónica García-Hernández,[‡] Alberto Domingo,[‡] Antonio L. Llamas-Saiz,[§] Silvia Porto-Sandá,[#] Ricardo Riguera,[#] William Laine,[∥] Marie-Hélène David-Cordonnier,[∥] Christian Bailly,[∥,●] Luis F. García-Fernández,[⊥] Juan José Vaquero,[∞] and Federico Gago*[,†]

Departamento de Farmacología, Departamento de Bioquímica y Biología Molecular, and Departamento de Química Orgánica, Universidad de Alcalá, E-28871 Madrid, Spain, Unidad de Rayos X, Laboratorio Integral de Dinámica y Estructura de Biomoléculas José R. Carracido, Edificio CACTUS, Campus Sur, Universidad de Santiago de Compostela, 15782 Santiago de Compostela, Spain, Departamento de Química Orgánica, Facultad de Química, Universidad de Santiago de Compostela, E-15706 Santiago de Compostela, Spain, INSERM U-524 and Laboratoire de Pharmacologie Antitumorale du Centre Oscar Lambret, IRCL, Place de Verdun, F-59045 Lille, France, and PharmaMar S.A., Avda. de los Reyes 1, Polígono Industrial La Mina-Norte, E-28770 Colmenar Viejo, Madrid, Spain

Received March 31, 2007

The marine natural product thiocoraline A displayed approximately equal cytotoxic activity at nanomolar concentrations in a panel of 12 human cancer cell lines. X-ray diffraction analyses of orthorhombic crystals of this DNA-binding drug revealed arrays of docked pairs of staple-shaped molecules in which one pendent hydroxyquinoline chromophore from each cysteine-rich molecule appears intercalated between the two chromophores of a facing molecule. This arrangement is in contrast to the proposed mode of binding to DNA that shows the two drug chromophores clamping two stacked base pairs, in agreement with the nearest-neighbor exclusion principle. Proof of DNA sequence recognition was obtained from both classical DNase I footprinting experiments and determination of the melting temperatures of several custom-designed fluorescently labeled oligonucleotides. A rationale for the DNA-binding behavior was gained when models of thiocoraline clamping a central step embedded in several octanucleotides were built and studied by means of unrestrained molecular dynamics simulations in aqueous solution.

Introduction

Thiocoraline A (Figure 1, hereafter thiocoraline) is an antitumor cyclic thiodepsipeptide isolated from the mycelium of a marine actinomycete, *Micromonospora* sp. L-13-ACM2−092,[1−3] that has been shown to exhibit exceptionally potent activity in the L1210 mouse leukemia cytotoxic assay (IC_{50} = 200 pM)[4] and to inhibit the elongation activity of DNA polymerase α in both LoVo and SW620 human colon cancer cells.[5] This latter mechanism was invoked to account for the observed arrest in the G1 phase of the cell cycle and the decrease in the rate of S phase progression toward G_2/M phases, given that this agent neither inhibits DNA topoisomerase II nor induces DNA strand breaks.

From a structural standpoint, thiocoraline belongs to a class of naturally occurring 2-fold symmetric or pseudosymmetric bicyclic octadepsipeptides that include the well-known quinoxaline antibiotics triostin A and echinomycin.[6] These two agents have been shown to unwind negatively supercoiled double-stranded DNA and to bind to DNA by bisintercalation,[7,8] which takes place preferentially around the cognate dinucleotide sequence CpG.[6] In contrast, for thiocoraline, despite the reported high-affinity bisintercalative DNA binding, little or no perceptible sequence selectivity has been detected so far.[4]

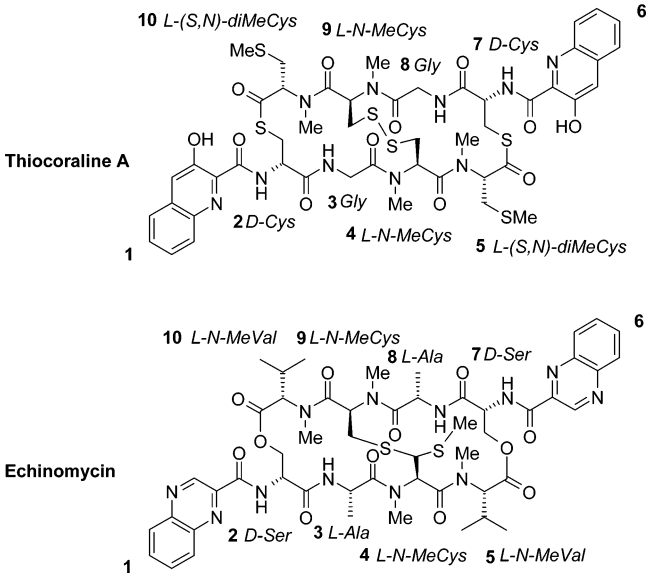

Figure 1. Chemical structures of thiocoraline A and echinomycin. Constituent amino acids are labeled in italics, and residue numbers are shown in bold. Note the symmetry-breaking thioacetal cross-linkage in echinomycin that replaces the disulfide bond present in 2-fold symmetric thiocoraline A and triostin A. 2QN is the bisquinoline derivative of echinomycin produced by directed biosynthesis. Thiocoraline is a cyclic depsipeptide made up of the following amino acids: two glycine units, two units of D-cysteine each presenting the sulfur atom as a thioester and the nitrogen forming an amide with the 3-hydroxyquinaldic acid, two units of *N*,*S*-dimethyl-L-cysteine with the carboxylic group as a thioester, and two units of *N*-methyl-L-cysteine linked to each other through a disulfide bond.

* To whom correspondence should be addressed. Telephone: +34-918 854 514. Fax: +34-918 854 591. E-mail: federico.gago@uah.es.
[†] Departamento de Farmacología, Universidad de Alcalá.
[‡] Departamento de Bioquímica y Biología Molecular, Universidad de Alcalá.
[§] Laboratorio Integral de Dinámica y Estructura de Biomoléculas José R. Carracido, Universidad de Santiago de Compostela.
[#] Departamento de Química Orgánica, Universidad de Santiago de Compostela.
[∥] INSERM U-524 and Laboratoire de Pharmacologie Antitumorale du Centre Oscar Lambret
[⊥] PharmaMar S.A.
[∞] Departamento de Química Orgánica, Universidad de Alcalá.
● Present address: Centre de Recherche en Oncologie Expérimentale (CROE), ISTMT, Parc Technologique du Canal, 3 Rue des Satellites BP 94244, 31432 Toulouse, France.

10.1021/jm070381s CCC: $37.00
Published on Web 06/16/2007

This finding is somewhat intriguing because, in common with these other natural compounds, thiocoraline possesses a D-stereochemistry (D-Cys) at the *R*-position of the amide linkage to the heteroaromatic intercalating chromophore and possesses L-stereochemistry at the remaining stereogenic centers.[9] On the other hand, although it incorporates the unusual D-Cys linked to 3-hydroxyquinaldic acid (as in sandramycin)[10] rather than to the quinoxalinic acid that is characteristic of triostin and echinomycin (Figure 1), a thiocoraline analogue bearing the quinoxaline chromophore of echinomycin was found to behave in a manner indistinguishable from that of thiocoraline itself.[11] The other structural features that make thiocoraline stand out from the rest of the group and could account for the reported abolition of its DNA binding selectivity are (i) the presence of a thioester in the depsipeptide backbone instead of an ester, (ii) the replacement of the standard $CH(CH_3)_2$ of *N*-methylvaline with a CH_2SCH_3 side chain, and (iii) the possibly more significant Gly versus L-Ala substitution.[4]

Thiocoraline has been shown to adopt a single solution conformation, as observed by ^{1}H NMR in well-defined spectra,[1,4] but neither the three-dimensional structure of this bifunctional DNA ligand nor structural details of its interaction with DNA have been reported. In the following, we describe (i) the X-ray crystal structure of thiocoraline, (ii) results on its DNA-binding preferences obtained from both standard DNase footprinting assays and DNA melting experiments using fluorescently labeled oligodeoxynucleotides of defined sequence,[12] and (iii) results of molecular modeling followed by molecular dynamics simulations of the bisintercalated complexes between thiocoraline and several octanucleotides containing some of its preferred target sites in their central region. Whenever possible, echinomycin and its bisquinoline analogue, 2QN,[a,13,14] have also been used for comparative purposes.

Results and Discussion

Cytotoxicity. Twelve diverse human cancer cell lines were used to evaluate the cytotoxic potential of thiocoraline. The disease-oriented screen included prostate (DU-145 and LN-CaP), ovary (IGROV), breast (SK-BR3), melanoma (SK-MEL-28), lung-NSCLC (A-549), leukemia (K-562), pancreas (PANC-1), colon (HT-29, LoVo, and LoVo-DOX, a subclone of LoVo cells overexpressing the drug efflux pump Pgp170) and cervix (HeLa). An adaptation of the sulforhodamine B (SRB) colorimetric assay[15] was set up to estimate GI_{50} values, i.e., the drug concentration needed to inhibit cell growth by 50% after 72 h of continuous exposure to the test molecule. As shown in Table 1, thicoraline displayed comparable antitumor potency in all the cell lines tested in terms of GI_{50} values, with a median of 2.4 ± 1.7 nM. More dissimilar results were obtained when other parameters such as TGI and LC_{50} were analyzed. K-562 and LNcaP cell lines were more sensitive, whereas HT-29, DU-145, and IGROV cells were less sensitive to thiocoraline. The least activity, by far, was detected on multidrug-resistant LoVo-Dox cells, which showed 87- and 215-fold increases in GI_{50} and TGI values, respectively, when compared to the median value of the complete cell panel. Furthermore, the LC_{50} was never reached in these cells within the concentration range used (10−0.016 μg/mL), strongly suggesting that thicoraline is a Pgp170/MDR substrate, and thus multidrug resistance should be a factor to be taken into account when its use is intended for therapeutic applications.

Table 1. Cytotoxic Activity of Thiocoraline A on Different Human Tumor Cell Lines[a]

cell line	cytoxic activity (nM)		cell line	cytoxic activity (nM)	
DU-145	GI_{50}	1.9	K-562	GI_{50}	1.3
	TGI	6.4		TGI	4.6
	LC_{50}	1481.3		LC_{50}	9.2
LN-CaP	GI_{50}	3.0	PANC-1	GI_{50}	2.5
	TGI	5.0		TGI	82.5
	LC_{50}	14.2		LC_{50}	378.0
IGROV	GI_{50}	1.9	HT-29	GI_{50}	3.9
	TGI	11.1		TGI	73.6
	LC_{50}	1257.1		LC_{50}	6293.3
SK−BR-3	GI_{50}	2.2	LoVo	GI_{50}	7.2
	TGI	8.9		TGI	263.1
	LC_{50}	30.8		LC_{50}	283.5
SK-MEL-28	GI_{50}	3.0	LoVo-Dox	GI_{50}	212.3
	TGI	14.0		TGI	2380.0
	LC_{50}	50.3		LC_{50}	nd
A-549	GI_{50}	4.8	HeLa	GI_{50}	1.3
	TGI	19.3		TGI	4.7
	LC_{50}	95.6		LC_{50}	22.6

[a] GI_{50}: drug concentration causing 50% growth inhibition. TGI: drug concentration causing total growth inhibition. LC_{50}: drug concentration causing 50% net cell killing. nd: not determined.

X-ray Crystal Structure and Absolute Stereochemistry. The crystal structure of thiocoraline is shown in Figure 2. ORTEP diagrams (Figures S1−S3) and crystal data (Tables S1−S8) can be found in the Supporting Information.

The known configurations of the six asymmetric centers[9] of the molecule were confirmed by the Flack parameter refinement (see experimental part): *R* for the two D-cysteines bonded to the 3-hydroxyquinaldic acid and *S* for the remaining L-amino acids. The two crystallographically independent molecules (A and B) present in the asymmetric unit of the unit cell have similar conformations (Supporting Information, Figures S4 and S5) and display a large 26-membered macrocycle with the disulfide bridge pointing to the convex side and the two quinoline units pointing in the opposite direction. The general appearance of the molecule is that of a (12,12,4)-bicycle with the disulfide bridge closer to one of the 12-membered rings for molecule A and in a more symmetrical fashion for molecule B; the distance separating the thioester sulfur atoms from those making up the disulfide bridge is 4.1−4.9 Å in one case and 7.0−7.7 Å (molecule A) or 5.3−6.5 Å/5.7−6.9 Å (molecule B) in the other one. The 3-hydroxyquinaldic acid moieties are placed on the concave side of the bicycle with their heteroaromatic rings on almost parallel planes (10.6° for molecule A and 23.1° for molecule B) but rotated 180°, that is, with the phenolic groups as far apart as possible (Figure 2 and Supporting Information). The separation between the planes of the two quinoline rings is 6.9 Å for both molecules, and the phenolic OH is hydrogen-bonded to the amide carbonyl in two of the rings.

In the crystal lattice, the thiocoraline molecules are docked in pairs in such a way that one of the quinoline rings from each molecule is sandwiched between the two rings of the facing molecule. These pairs, in turn, form infinite columns along the *c*-axis of the crystals because the outer rings of each pair are stacked in antiparallel orientation onto their symmetry equivalents from neighboring molecules (Figure 2). The mean distances between the stacked aromatic rings are in the range 3.4−3.7 Å.

[a] Abbreviations: 2QN, the bisquinoline derivative of echinomycin; TANDEM, des-*N*-tetramethyltriostin A; SRB, sulforhodamine B; T_m, melting temperature; K_d, dissociation constant; C_{50}, half-maximal change in melting temperature; GI_{50}, compound concentration that produces 50% inhibition on cell growth; TGI, compound concentration that produces total growth inhibition; LC_{50}, compound concentration that produces 50% net cell killing; MEP, molecular electrostatic potential; MD, molecular dynamics; HRE, hypoxia-responsive element; VEGF, vascular endothelial growth factor.

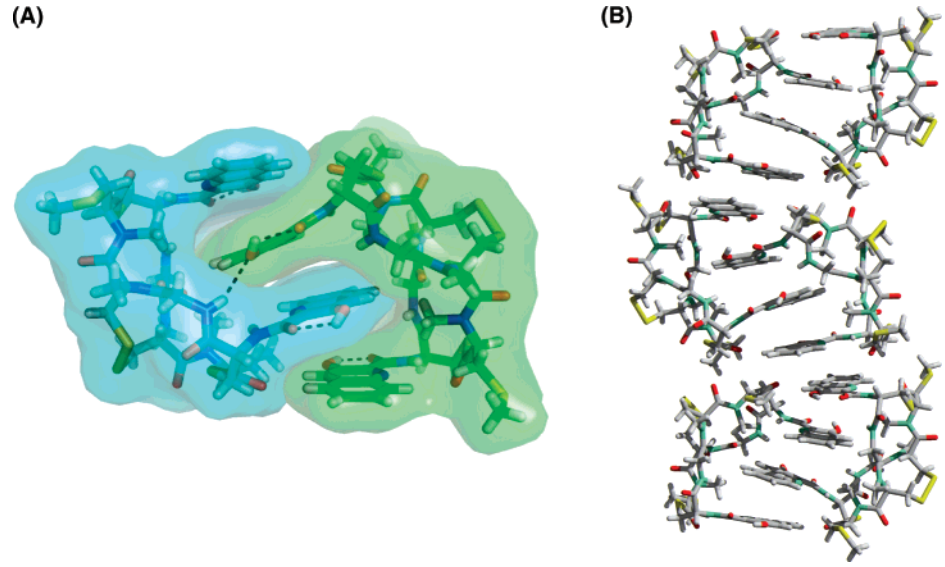

Figure 2. (A) Reciprocal docking of two thiocoralines molecules in the asymmetric unit of the unit cell of the crystal solved by X-ray crystallography. The hydrogen bond between the glycine amide nitrogen of one molecule and the hydroxyl oxygen on the quinaldic moiety of the facing molecule is displayed as a dashed line. (B) Stacked array of these mutually clamped thiocoraline molecule pairs along the *c*-axis of the crystal. Sulfur, oxygen, and nitrogen atoms are colored yellow, red, and cyan, respectively.

There are many weak hydrogen-bonding interactions of the kind C−H···X, where X is O, S, Cl, or π-ring electron density, that account for the global packing of the structure (Supporting Information, Figures S6−S8). This packing arrangement is novel for bisintercalators because it is not present in any of the crystal structures deposited in the Cambridge Structural Database,[16] namely, triostin A,[17,18] des-*N*-tetramethyltriostin A (TANDEM),[19] and the bisquinoline derivative of echinomycin, 2QN.[17]

Since the two heteroaromatic rings are orientated approximately perpendicular to the thiodepsipeptide ring, the molecule resembles the familiar staple shape of quinoxaline antibiotics represented by triostin A and echinomycin and also that of related natural antineoplastic agents such as sandramycin[10] and luzopeptin.[20] This finding strongly suggests that thiocoraline employs the same mechanism of bisintercalation for binding to DNA.

DNA Footprinting. Overall, the footprints produced upon digestion of a radiolabeled 117 base pair (bp) restriction fragment from plasmid pBS with DNase I following incubation with thiocoraline were roughly superimposable, but not identical, to those observed in the presence of echinomycin and/or 2QN (Figure 3). For example, the 5′-ACGTCGT/ACGACGT sequence at positions 49−55, which provides two adjacent but mutually exclusive CpG sites for echinomycin and 2QN (underlined), did not afford a good binding site for thiocoraline even though some protection was apparent around position 50 at the highest concentration (Figure 4). Likewise, the ACGC site centered around position 74, which is protected by echinomycin at both concentrations and 2QN only at the higher concentration, was indifferent to the presence of thiocoraline. This lack of protection at some ACGX sites was not absolute, however, because a clear binding site for thiocoraline could be seen at the bottom of the gel around position 21 corresponding to the sequence 5′-TCGT/ACGA. On the other hand, the 5′-CCGT/ACGG sequence preceding a short A-tract at positions 36−39, which is protected from DNase I by 2QN on the 3′-side and even more strongly by echinomycin on the 5′-side, appeared to bind thiocoraline in a similar way compared to the latter compound. In this respect, it is noteworthy that monoquinoline and bisquinoline analogues of echinomycin[14] have been shown to exhibit comparable but not identical patterns of DNA binding preferences to that seen with the parent compound.[13,21,22]

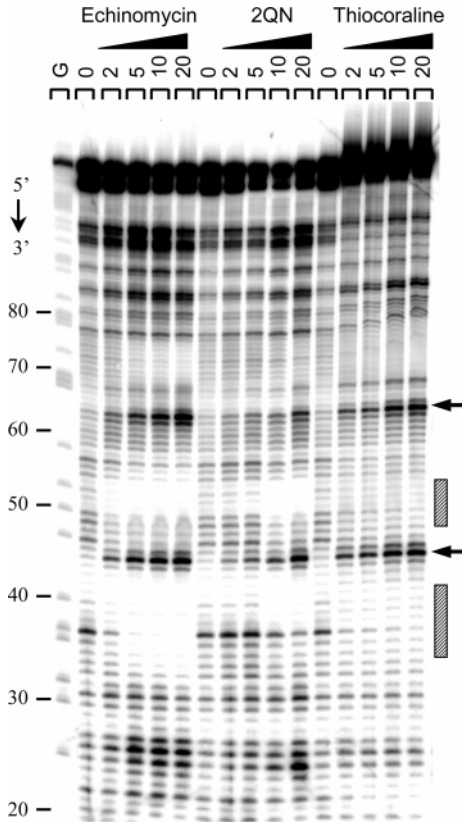

Figure 3. DNase I footprinting showing sequence-selective binding thiocoraline, echinomycin, and 2QN. The 117-bp *Eco*RI-*Pvu*II restriction fragment from plasmid pBS was 3′-end-labeled at the EcoRI site with [α-^{32}P]dATP in the presence of AMV reverse transcriptase. The products of the DNase I digestion were resolved on an 8% polyacrylamide gel containing 8 M urea. Drug concentrations are indicated at the top of the lanes. Control tracks (marked 0) contained no drug. Guanine-specific sequence markers obtained by treatment of the DNA with dimethylsulfate followed by piperidine were run in the lane marked G. Numbers on the left side of the gels refer to the standard numbering scheme for the nucleotide sequence of the DNA fragment.

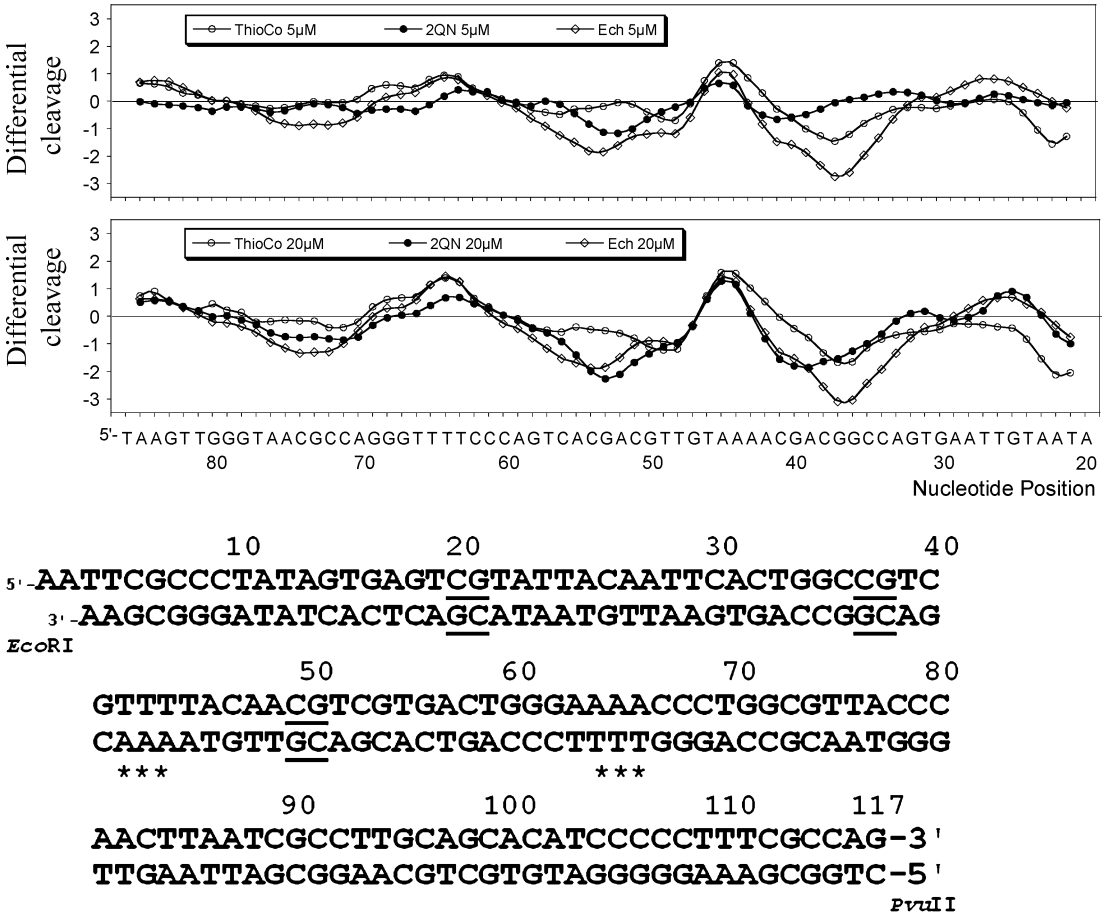

Figure 4. (Top) Differential cleavage plots comparing the susceptibility of the 117-bp DNA fragment to DNase I cutting in the presence of thiocoraline, echinomycin, and 2QN at the indicated concentrations. Negative values correspond to a ligand-protected site, and positive values represent enhanced cleavage. Vertical scales are in units of $\ln(f_a) - \ln(f_c)$, where f_a is the fractional cleavage at any bond in the presence of the drug and f_c is the fractional cleavage of the same bond in the control, given closely similar extents of overall digestion. Each line drawn represents a three-bond running average of individual data points, calculated by averaging the value of $\ln(f_a) - \ln(f_c)$ at any bond with those of its two nearest neighbors. Only the region of the restriction fragments analyzed by densitometry is shown. (Bottom) Complete sequence of the 117-bp restriction fragment, with the positions of the main footprints underlined and the sites of enhanced cleavage marked with asterisk.

In addition to the sites of protection from DNase I digestion, there are also several sites where cleavage was enhanced, in particular within the AT tracts at positions 45 and 63. Unlike the footprints, the enhancement at these two sites was equally pronounced in the thiocoraline and echinomycin lanes, possibly suggesting that these two antibiotics perturb the structure of the DNA double helix to a comparable extent so that access of the nuclease to the minor groove of AT-rich sequences is equally facilitated. Taken together, these results hint at some clear preference for CpG steps irrespective of the nature of the flanking bases in contrast to some earlier reports that thiocoraline binds to DNA with hardly any sequence selectivity. It must be noted, however, that this claim was made on the basis of both footprinting experiments using w794 DNA and apparent binding constants calculated from titration of the drug with either calf thymus DNA or a set of just four short duplex oligodeoxynucleotides of general formula 5′-GCXYGC-3′, where XY = TA, AT, GC, or CG.[4]

Fluorescence Melting Studies. To validate and possibly expand the findings reported above, the ability of thiocoraline to stabilize the double helical structure of several fluorophore-labeled oligodeoxynucleotides ("molecular beacons") of widely different base-pair compositions (Table 2) was studied using fluorescence measurements. This method allows the rapid, inexpensive, and reproducible determination of highly accurate melting profiles in parallel using microliter samples each containing very small amounts of well-defined DNA and increasing concentrations of a DNA-binding ligand (see methodology section). By use of a decision tree for the choice of oligos, the selected DNA sequences can be used to explore from the very initial A−T vs G−C broad preferences down to more subtle effects brought about by flanking base pairs or sequence context.

Thus, the duplex containing the A−T rich sequence, AT, produced a simple monophasic profile with a melting temperature (T_m) of 44 °C that changed only slightly upon addition of increasing concentrations of thiocoraline. In fact, at a drug concentration of 20 μM, the ΔT_m reached a maximum of only ~6 °C. In contrast, the T_m of the G−C rich oligo, GC, steadily increased upon addition of thiocoraline, and the melting curve was shifted by almost 18 °C at the same concentration of 20 μM (Figure 5). This striking difference, which was equally apparent for the better characterized and CpG-binding echinomycin, appears to suggest a preference of thiocoraline for DNA sequences rich in G−C base pairs much more clearly than previously reported.[4] Furthermore, comparable extents of duplex stabilization were achieved at concentrations of thiocoraline about 10 times lower than those of echinomycin (cf.

Table 2. Sequences of the Fluorescently Labeled Oligonucleotides Employed in the Melting Temperature Experiments

name	sequence
AT	5′-F-CAATTAAATATAAC-3′ 3′-Q-GTTAATTTATATTG-5′
GC	5′-F-GCGCGGCGTCCGGGCC-3′ 3′-Q-CGCGCCGCAGGCCCGG-5′
ACCA	5′-F-AATATAAACCAAATTAA-3′ 3′-Q-TTATATTTGGTTTAATT-5′
AGCA	5′-F-AATATAAAGCAAATTAA-3′ 3′-Q-TTATATTTCGTTTAATT-5′
ACGA	5′-F-AATATAAACGAAATTAA-3′ 3′-Q-TTATATTTGCTTTAATT-5′
2SS	5′-F-AATATACGTAATATCGATTAA-3′ 3′-Q-TTATATGCATTATAGCTAATT-5′
2AS	5′-F-AATATACGTTCGATTAA-3′ 3′-Q-TTATATGCAAGCTAATT-5′
ACGT	5′-F-AATATAAAACGTTAAATTAA-3′ 3′-Q-TTATATTTTGCAATTTAATT-5′
TCGA	5′-F-AATATAAATCGATAAATTAA-3′ 3′-Q-TTATATTTAGCTATTTAATT-5′
GCGC	5′-F-AATATAAAGCGCTAAATTAA-3′ 3′-Q-TTATATTTCGCGATTTAATT-5′
CCGG	5′-F-AATATAAACCGGTAAATTAA-3′ 3′-Q-TTATATTTGGCCATTTAATT-5′
GCGG	5′-F-AATATAAAGCGGTAAATTAA-3′ 3′-Q-TTATATTTCGCCATTTAATT-5′
GCGT	5′-F-AATATAAAGCGTTAAATTAA-3′ 3′-Q-TTATATTTCGCAATTTAATT-5′
ACGG	5′-F-AATATAAAACGGTAAATTAA-3′ 3′-Q-TTATATTTTGCCATTTAATT-5′

Table 3. Parameters Characterizing the Binding of Thiocoraline and Echinomycin to the Different Oligonucleotides Studied[a]

oligonucleotide	max ΔT_m [b] (°C)	C_{50} [c] (μM)	oligonucleotide	max ΔT_m [b] (°C)	C_{50} [c] (μM)
A. Thiocoraline					
2AS	23.0	0.71	ACCA	7.1	1.60
2SS	19.3	0.93	GCGG	6.7	0.39
GC	17.3	0.78	CCGG	6.7	0.49
ACGG	10.6	0.79	GCGT	6.7	0.31
ACGA	9.4	0.55	GCGC	6.1	0.59
ACGT	9.0	0.31	AT	5.7	0.57
TCGA	8.2	0.46	AGCA	2.9	1.74
B. Echinomycin					
2SS	24.7	1.22	TCGA	9.9	1.94
2AS	21.0	1.67	ACCA	9.4	3.0
GC	16.0	1.44	AGCA	6.9	3.79
ACGA	14.5	2.24	AT	6.0	3.96
ACGT	12.6	1.63			

[a] Tabulated in decreasing order of duplex stabilization for each drug. [b] The maximum increment in melting temperature with respect to the same oligonucleotides in the absence of drug. [c] The C_{50} value represents the half-maximal change in melting temperature.

the leftward shift of the curves), which suggests a tighter drug−DNA association.

To define the sequence preferences still further, an exploratory series of duplex oligodeoxynucleotides was designed (Table 2) and studied using the same methodology. First, the oligos TGGT/ACCA, AGCA/TGCT, and ACGA/TCGT addressed the issue of whether single GpG/CpC, GpC, or CpG steps were preferred. As seen in Figure 6, the last oligo was significantly more stabilized by both thiocoraline and echinomycin, which suggests a preference for the CpG step that is in accordance not only with the selectivity reported above from the footprinting data but also with previous experiments carried out with other bisintercalating antibiotics such as triostin A, echinomycin,[23] and 2QN.[21,22] Subsequently, a single central CpG step was embedded in different symmetrical and nonsymmetrical sequence contexts to produce the oligos ACGT, TCGA, GCGC, CCGG, GCGG, and GCGT, which were used to assess the influence of the base pairs flanking the putative bisintercalation site. Significant differences in duplex stabilization brought about by thiocoraline binding (Table 3) were also observed in this second series (Figure 7), with the nonsymmetrical ACGG (10.6 °C) and the symmetrical GCGC (6.1 °C) displaying the largest and smallest maximum increases in T_m, respectively. Taken together, these results appear to indicate that flanking sequences also have some bearing on the sequence selectivity of thiocoraline, in good consonance with the more limited footprinting data, with sites possessing an A on the 5′ side being more stabilized, and this is also true for echinomycin. For this latter drug, the greater ΔT_m for ACGT compared to TCGA is in nice agreement with earlier results showing faster dissociation kinetics from TCGA than from ACGT when the CpG site is found in an alternating AT environment[24] whereas the effect on ACGA is more concentration-dependent. The most striking difference between the profiles obtained for these two drugs, however, lies in the fact that a ΔT_m plateau is reached for thiocoraline at the highest concentrations tested but not for echinomycin. This finding possibly underscores a greater potential for nonspecific binding of this latter drug at high concentrations.

Although the largest stabilization was achieved with the GC oligonucleotide, it must be noted that at least three putative binding sites are present in this sequence, two of which do not overlap and therefore are not mutually exclusive. To assess the extra stabilization brought about by binding to two independent sites more accurately, two more oligos containing a pair of suitably spaced CpG steps were designed and assayed: 2SS, which contained one favorable ACGT site and another favorable TCGA site separated by an intervening AATA sequence; 2AS,

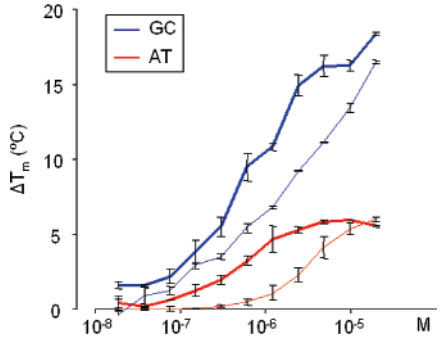

Figure 5. Effect on the DNA melting temperatures of fluorescently labeled AT and GC duplexes upon addition of increasing concentrations (logarithmic scale) of either thiocoraline (thick lines) or echinomycin (thin lines). For each point the error bars are centered on the average value of three independent measurements.

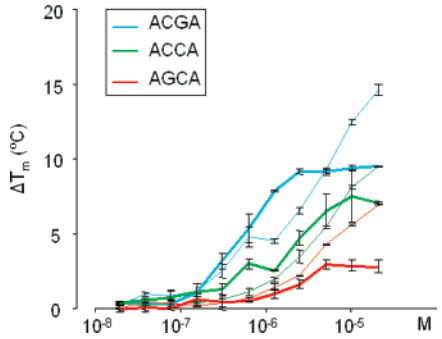

Figure 6. Melting temperature increments brought about by thiocoraline (thick lines) and echinomycin (thin lines) binding to TGGT/ACCA, AGCA/TGCT, and ACGA/TCGT duplexes.

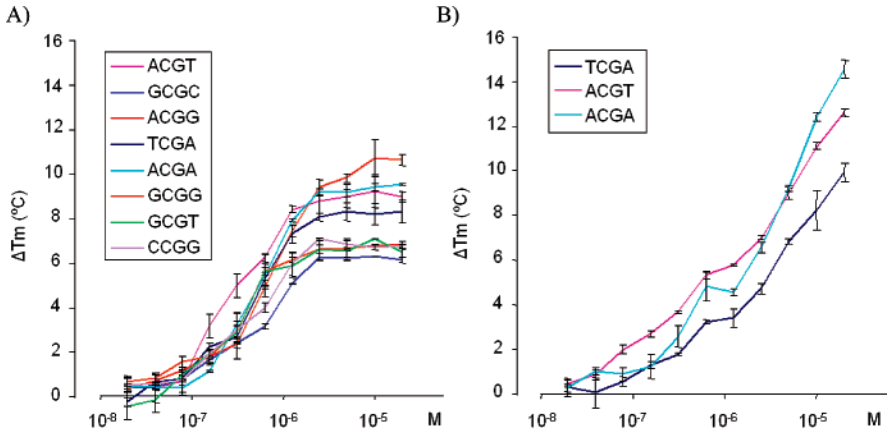

Figure 7. Melting temperature increments brought about by (A) thiocoraline or (B) echinomycin binding to a variety of oligodeoxynucleotides containing a CpG step embedded in different sequence contexts.

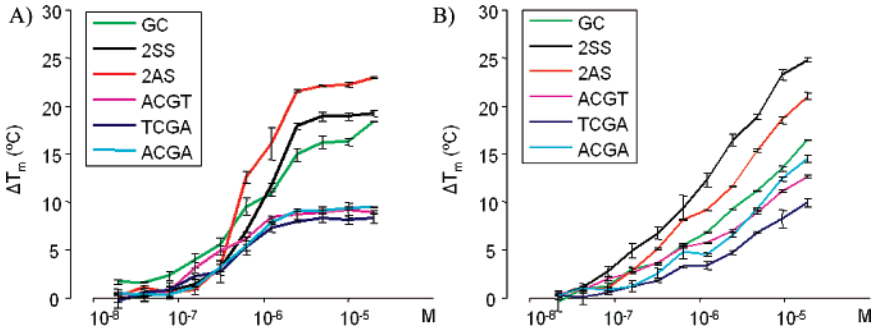

Figure 8. Fluorescence melting curves comparing duplex dissociation of the oligodeoxynucleotides containing a single binding site to those containing two separate or adjacent binding sites in the presence of increasing concentrations of (A) thiocoraline or (B) echinomycin.

which contained the same two sites adjacently disposed (Table 2). As clearly seen in Figure 8, the binding of two thiocoraline molecules to two independent and nonoverlapping sites resulted in greatly increased DNA stabilization that was even more pronounced in the oligo with the juxtaposed binding sites (Table 3), possibly hinting at cooperativity. Positive cooperativity has indeed been demonstrated in some cases for the better characterized echinomycin, and its extent has been shown to depend, using quantitative footprinting,[25] on the nature of the sequences clamped by the antibiotic and to diminish as the distance between the binding sites is increased. When the same oligodeoxynucleotides employed to probe the sequence specificity of thiocoraline were used for echinomycin, strikingly similar results were obtained (Figure 8), the major difference being found (the continuously raising slopes as reported above for other sequences notwithstanding) in the reverse order of stabilization for 2AS and 2SS. Once again, thiocoraline was able to stabilize the duplex to a greater extent than echinomycin at equivalent submicromolar concentrations, which again argues in favor of stronger binding for the former antibiotic.

At all concentrations, the melting profiles showed simple monophasic transitions, which are indicative that the bound and the free ligand are in rapid exchange.[38] It can be seen that upon incubation with either thiocoraline or echinomycin a concentration-dependent increase in fluorescence is produced that is related to the delay in the duplex → single-strand transition (Figure 9). Nonetheless, it is important to realize that we are not directly measuring binding affinities and/or occupancies using this method. Rather, the presence of the drug stabilizes the duplex, thus shifting the equilibrium between single-stranded and double-stranded DNA at each temperature in favor of the latter. It is this population redistribution that is translated into the measured changes in fluorescence. Therefore, fitting of the

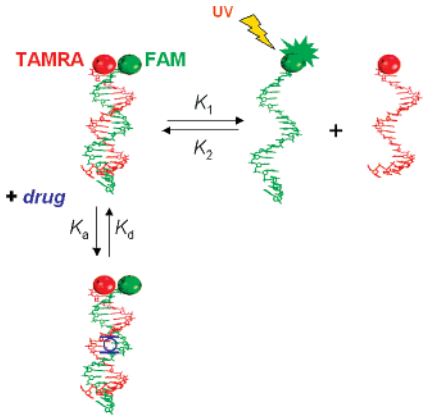

Figure 9. Schematic of a typical melting experiment using fluorescently labeled oligonucleotides. The DNA double helix dissociates into two single strands upon melting at a given temperature (T_{m1}) that depends on nucleotide composition and sequence. The equilibrium (and fluorescence) at each temperature is governed by the kinetic rate constants K_1 and K_2. A DNA-binding ligand (blue molecule) with a unique affinity for this oligo in the duplex state determined by the magnitude of its association and dissociation constants K_a and K_d, respectively, will shift the former equilibrium toward this state, thus hampering strand separation, which brings about the observed increment in melting temperature in the presence of drug (T_{m2}). The ΔT_m values reported in Table 3 and Figures 5−8 correspond to $T_{m2} - T_{m1}$. Drug dissociation from DNA takes place in a single-step reaction,[24] which implies that both chromophores are simultaneously withdrawn from the DNA lattice.

data to a simple rectangular hyperbola allows one to approximate a value for the half-maximal change in melting temperature, C_{50}, for each oligo (provided a plateau has been reached), but this quantity lacks any direct physical meaning. Indirectly, however, C_{50} values can be related to the dissociation constants

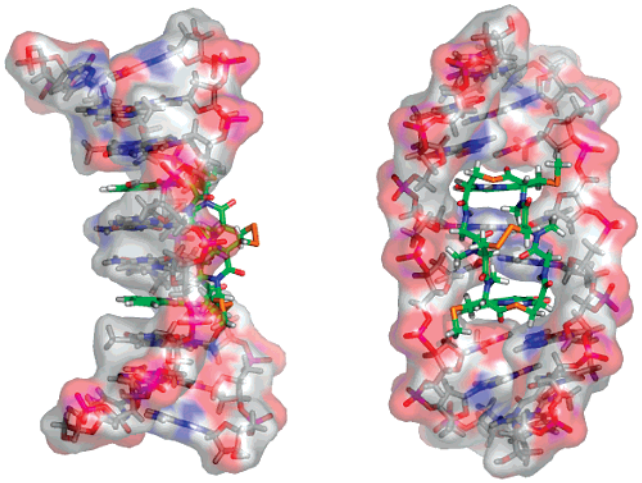

Figure 10. Side and front views of a representative structure of the bisintercalated thiocoraline-d(CATCGTG)$_2$ complex studied. Note the unwinding of the helix that is typical in the complexes of echinomycin and triostin A with similar oligonucleotides.[8,30] DNA atoms are enveloped by a semitransparent surface, and thiocoraline is displayed as sticks with C atoms colored in green.

(K_d) of the ligands and used to compare their binding affinities when the same DNA molecule is used, as shown here for thiocoraline and echinomycin. Since the former drug needs ~10-fold lower concentrations to give rise to a similar DNA stabilization, especially at submicromolar concentrations, it can be surmised that its binding affinity is about 1 order of magnitude larger. On the other hand, the differences in ΔT_m calculated for the different oligonucleotides in the presence of equivalent concentrations of the same ligand reflect the varying extents of duplex stabilization brought about by ligand binding, which is also proportional to the K_d of the ligand insofar as this constant affects the equilibrium between single- and double-stranded DNA at each temperature (Figure 9). Therefore, the maximum ΔT_m values reported in Table 3 constitute a convenient means of comparing the relative affinities of either thiocoraline or echinomycin for the different sequences. It must be noted, however, that ΔT_m and C_{50} values are not correlated because of intrinsic differences in the T_m and association/dissociation rate constants (K_1, K_2) for the oligos. The validity of this reasoning is substantiated by the good correspondence between the results obtained for echinomycin using the fluorescence melting method and accumulated data from footprinting, NMR, and X-ray crystallographic evidence. In fact, even the relatively minor stabilization imparted on the AT or ACCA oligonucleotides by these bisintercalating ligands is consistent with some secondary and weaker binding sites previously reported for echinomycin.[26]

Molecular Dynamics Simulations. In light of the previous findings, we modeled and simulated the dynamic behavior of the complexes of thiocoraline with several octanucleotides containing 5′-ACGT-3′, 5′-ACGA-3′, 5′-TCGA-3′, and 5′-ACCA-3′ core sequences. The former three DNA molecules were also studied in complex with echinomycin, which is known to bind with high affinity to these sites.[6]

The conformation of thiocoraline in the crystal structure reported above implies a high degree of structural preorganization for DNA binding. Nonetheless, some structural rearrangements are still necessary to widen the distance between the two chromophores (from ~6.8 to ~10.2 Å) in order to clamp two DNA base pairs in place of a single heteroaromatic ring from the facing molecule. On the other hand, the unwound DNA (Figure 10) must comply with the nearest-neighbor exclusion principle to permit bisintercalation and thus resemble the conformation found in the complexes with echinomycin and similar bisintercalators.[27]

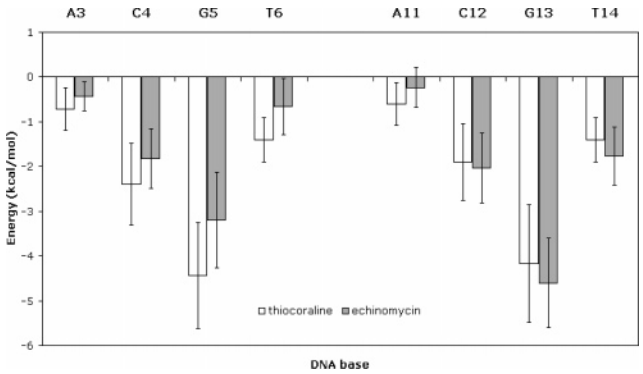

Figure 11. Calculated electrostatic interaction energies between either thiocoraline (white bars) or echinomycin (shaded bars) and the DNA bases that make up the two intercalation sites in the ACGT octanucleotide studied. These results are mean values ± standard deviation (kcal mol^{-1}) from snapshots taken every 2.0 ps from the 2 ns production phase of the MD simulations.

The quinoline rings clamp the central two base pairs, and the complexes are stabilized by three major factors: (i) van der Waals interactions between the sulfur-rich peptide part of the antibiotic and the minor grooves of the oligomers, (ii) stacking interactions between the quinoline rings and the adjacent base pairs, and (iii) hydrogen-bonding interactions between the NH and carbonyl groups of glycines and between the N3 and 2-amino groups of guanines. For echinomycin these hydrogen bonds involving the alanine residues have been shown to be essential for the specific binding to CpG steps,[28] which accounts for the selective pattern of DNase cleavage inhibition mostly centered around one or more of these cognate steps (Figure 4).

The pattern of hydrogen bonds between the depsipeptide residues of echinomycin and the central base pairs points to the simultaneous occurrence of only three hydrogen bonds, a finding that is in consonance with previous NMR[29] and X-ray[8] results. In contrast, for thiocoraline, four hydrogen bonds are concurrently maintained during the whole length of the simulation in the CpG-containing duplexes (Table 4) most likely because of the removal of the two methyl groups facing the DNA minor groove upon replacement of each alanine residue with a glycine (Figure 1). This finding, together with an increase in the hydrophobic effect, could account for the apparently greater affinity of thiocoraline relative to echinomycin. Nonetheless, in the complex of thiocoraline with the nonsymmetrical CpC/GpG-containing octanucleotide (representative of the oligo that was weakly but significantly stabilized in the fluorescence melting experiments), only three hydrogen bonds are systematically observed. This finding underscores the optimal arrangement of hydrogen bond donor and acceptor groups in CpG relative to CpC/GpG steps for thiocoraline (and echinomycin) binding.

The most prominent DNA structural alteration in the complexes studied is helix unwinding (Figure 10), which takes place to a similar extent irrespective of the type of drug and sequence context (data not shown). Other DNA architectural parameters such as the rise of each base pair along the helical axis, which is increased at both intercalation sites by about 4.2 Å, and the ensuing buckling of the inner G−C base pairs clamped by the intercalating moieties of the drugs are also similar in the echinomycin and thiocoraline complexes studied (data not shown). These features have been extensively documented in the past for several DNA complexes of quinoxaline antibiotics

Table 4. Intermolecular Hydrogen-Bonding Donor−Acceptor Distances (Å) and Angles (deg) between DNA and Either Thiocoraline or Echinomycin in the Different Modeled Complexes Studied[a]

	ACGA−thiocoraline		ACGT−thiocoraline		TCGA−thiocoraline		ACCA−thiocoraline	
	distance (Å)	angle (deg)	distance (Å)	angle (deg)	distance (Å)	angle (deg)	distance (Å)	angle (deg)
N2−G5/O−Gly3	3.2 ± 0.3	161.3 ± 9.0	3.2 ± 0.3	161.9 ± 8.5	3.2 ± 0.3	161.9 ± 8.7		
N3−G5/NH−Gly3	3.0 ± 0.1	141.5 ± 10.0	3.0 ± 0.1	143.1 ± 10.1	3.0 ± 0.1	140.9 ± 10.5		
N2−G13/O−Gly8	3.1 ± 0.3	163.8 ± 8.0	3.1 ± 0.2	163.1 ± 8.7	3.1 ± 0.3	163.3 ± 8.5		
N3−G13/NH−Gly8	3.1 ± 0.2	137.6 ± 10.0	3.0 ± 0.1	138.4 ± 10.3	3.1 ± 0.2	136.6 ± 9.8		
O2−C5/NH−Gly3							2.9 ± 0.2	131.2 ± 14.3
N2−G12/O−Gly3							*3.5 ± 0.4*	*136.6 ± 8.4*
N2−G13/O−Gly8							3.1 ± 0.2	161.6 ± 8.9
N3−G13/NH−Gly8							3.0 ± 0.2	139.6 ± 11.3

	ACGA−echinomycin		ACGT−echinomycin		TCGA−echinomycin	
	distance (Å)	angle (deg)	distance (Å)	angle (deg)	distance (Å)	angle (deg)
N2−G5/O−Gly3	2.9 ± 0.2	162.5 ± 8.7	2.9 ± 0.1	164.0 ± 8.2	3.1 ± 0.2	158.2 ± 9.6
N3−G5/NH−Gly3	*3.6 ± 0.4*	*118.4 ± 20.6*	*3.7 ± 0.3*	*109.2 ± 17.5*	3.1 ± 0.2	136.1 ± 11.2
N2−G13/O−Gly8	3.0 ± 0.2	159.3 ± 9.8	3.1 ± 0.2	159.0 ± 9.1	3.0 ± 0.2	159.2 ± 10.4
N3−G13/NH−Gly8	3.1 ± 0.2	135.4 ± 12.4	3.1 ± 0.2	135.3 ± 12.1	*3.8 ± 0.4*	*109.8 ± 15.9*

[a] Distances and angles shown in italics are given only for comparative purposes because they do not correspond to bona fide hydrogen bonds.

including those obtained from the highest resolution X-ray crystal structures[30] and from molecular dynamics simulations.[31]

As proposed for echinomycin,[32] the 2-carboxamide group attached to each of the heteroaromatic ring systems of thiocoraline does participate in the stacking interactions between the intercalating chromophores and the DNA bases because of the coplanarity brought about by conjugation. This is even more true in the case of thiocoraline for which a tricycle can be considered the actual intercalating moiety because of the additional virtual ring resulting from the hydrogen bond established between the 3-hydroxy group on the quinoline and the neighboring carboxamide oxygen. The stacking overlap of the chromophores, as is usually the case for this type of complexes, is comparatively larger relative to the base pairs external to the bisintercalation sites than relative to the internal bases.

Electrostatic interactions between the drugs and the core DNA sequences were estimated by means of Poisson−Boltzmann calculations, as previously reported. Figure 11 shows the results obtained for the complexes of thiocoraline and echinomycin with a representative ACGT duplex. These values include the interaction of the depsipeptide with the minor groove as well as the electrostatic component of the stacking interactions between the quinoline or quinoxaline rings of the bisintercalators and the adjacent base pairs. It can be seen that the magnitude of these interactions is very similar for both complexes, the largest contribution arising from the two G−C base pairs clamped by the drugs and the major difference being related to the asymmetry of hydrogen bonds in the case of echinomycin (cf. G5 vs G13). Taken together, the calculations support the view that both drugs use a very similar electrostatic mechanism for DNA recognition and binding.

Since the fluorescence melting experiments revealed an unanticipated significant stabilization of the ACCA duplex by thiocoraline (and echinomycin), we also compared the results obtained for ACGA- and ACCA-containing octanucleotides. The exchanges of G5 for C5 and C12 for G12 result in the repositioning of the hydrogen-bonding amino group in the minor groove for the second GC−base pair and loss of one hydrogen bond (Table 4). Although this relocation does not significantly affect the electrostatic interaction energy with the former base, the swap is clearly deleterious for the latter, which may account for the decreased affinity of ACCA relative to ACGA.

Biological Implications. Echinomycin (NSC-13502) has been recently shown to specifically inhibit binding of the transcription factor HIF-1 (hypoxia-inducible factor-1) to the endogenous hypoxia-responsive element (HRE) of the vascular endothelial growth factor (VEGF) promoter.[33] Genes controlled by HIF-1 encode proteins that are involved in crucial aspects of cancer biology, including cell survival, glycolysis, angiogenesis, migration, and invasion.[34] Interestingly, the VEGF promoter contains the core sequence 5′-R(A/G)CGTG-3′, which affords a good binding site for both echinomycin and thiocoraline (underlined). We also note that a similar good binding site for these drugs is present in a conserved sequence motif termed the downstream promoter element, (A/G)G(A/T)CGTG, which is found near the transcription start site of many TATA-box-deficient (TATA-less) core promoters and is highly conserved from *Drosophila* to humans,[35] providing a recognition site for the RNA polymerase II basal transcription factor D (TFIID).[36] In fact, a search in the human promoter database (http://zlab.bu.edu/~mfrith/HPD.html) revealed numerous occurrences of ACGT and related sequences that we have shown offer good binding sites for both thiocoraline and echinomycin, also including combinations of adjacent sites such as TCGAACGAACGT. The issue of whether thiocoraline exerts its potent antiproliferative action through binding to crucial promoter sites in the genome is worth examining but beyond the scope of the present investigation. In any case, the results reported here support the view that thiocoraline binding to cellular DNA can prevent strand separation and lead to stalled transcription and replication forks particularly at sequences offering multiple adjacent binding sites.

Conclusions

The X-ray crystal structure of thiocoraline has revealed uniquely stacked arrays of cross-docked pairs of staple-shaped molecules that are highly preorganized for DNA binding through intercalation, although they still need to adapt to the geometric restrictions (nearest-neighbor exclusion) imposed by the bisintercalation binding mode.

Earlier attempts to establish a selectivity of DNA binding by titration using fluorescence quenching or DNase I and hydroxyl radical footprinting on w794 DNA failed to reveal a distinguishable selectivity for thiocoraline,[4] although a small preference was observed for GC-rich sequences.[11] We now show results from footprinting on a different DNA fragment, as well as fluorescence melting experiments using several short DNA duplexes, that unambiguously demonstrate clear binding preferences for this natural antineoplastic agent that are highly similar to those of the well-studied quinoxaline antibiotic echinomycin.

Compared to other techniques based on UV melting curves of mixed sequence DNAs, the fluorescent method reported in the present investigation requires very small amounts of sample and shows a large signal-to-noise ratio using standard real-time polymerase chain reaction (PCR) instrumentation. In addition, the custom-designed oligonucleotides provide a wealth of distinct and unique binding sites that are not usually present simultaneously in the plasmid DNA fragments typically employed in the footprinting experiments (unless a "universal substrate" is used)[37] or do not produce clear footprints,[24] thereby allowing for a considerable expansion of the repertoire of discrete binding sites that can be tested in the search for the "optimal binding site". This nonradioactive technique has been previously used to measure the melting profiles of intramolecular DNA duplexes, triplexes, and quadruplexes[12] and also to characterize the DNA minor groove binding ligand thiazotropsin A,[38] but to the best of our knowledge this is the first time that it has been successfully applied to a bisintercalator that shows nanomolar potency as an antitumor agent against a diverse panel of human cancer cells.

The 3-hydroxyquinaldic system present in thiocoraline ensures a tricyclic hydrogen-bonded conformation that allows the antibiotic to intercalate into DNA and establish four good hydrogen bonds between its thiodepsipeptide and the minor groove of GC-rich sequences and particularly those encompassing a central CpG step. The molecular modeling results suggest that the DNA binding differences observed for the two drugs studied mostly result from the fact that the alanine residues in echinomycin are replaced with glycine in thiocoraline, which translates into the removal of two methyl groups that are found to be in close contact with the deoxynucleotide sugars and restrict the torsional freedom of this amino acid.

Materials and Methods

Drugs. Thiocoraline A was isolated and purified by PharmaMar, S.A. (Colmenar Viejo, Madrid, Spain), as described previously.[1] Echinomycin was purchased from Sigma-Aldrich, and 2QN was a generous gift to C.B. from Dr. Michael J. Waring (Cambridge University, U.K.).

X-ray Diffraction. Samples of 10−15 mg of thiocoraline were dissolved, filtered, and kept at room temperature. When acetonitrile was used as the solvent, an amorphous powder was obtained. Dissolution in acetone or trichloromethane resulted in oil formation and lack of crystals. Colorless single crystals were successfully obtained in dichloromethane and ethyl acetate, although many samples had to be rejected because of crystal association or very weak diffraction of the monocrystals due to structure decomposition and/or destruction of the crystalline lattice because of solvent loss. A suitably diffracting crystal ($0.60 \times 0.60 \times 0.60$ mm^3) that was grown by slow evaporation at room temperature from a solution containing 15 mg of thiocoraline in 2 mL of dichloromethane was finally selected and mounted on a Nonius MACH3 diffractometer coated with an amorphous polymer to minimize crystal decomposition. Diffraction data were measured at 293(2) K using graphite-monochromated Mo Kα (0.710 73 Å) radiation. The crystal symmetry corresponds to the orthorhombic space group $P2_12_12_1$ (No. 19). Unit cell dimensions were determined from 25 reflections ($9.2° < \theta < 11.0°$): $a = 20.804(4)$ Å, $b = 23.352(4)$ Å, $c = 25.974(5)$ Å, $V = 12618(4)$ Å^3, $Z = 4$, $D_c = 1.421$ g/cm^3, $F(000) = 5624$. The Friedel pair of every reflection was measured just after the intensity of each reflection was obtained to reduce errors in anomalous scattering differences due to crystal decay (7% during 17 days of data collection). Semiempirical absorption correction based on the ψ-scan method[39] was applied. The structure was solved by direct methods with SIR2004[40] and refined using full-matrix least-squares on F^2 with SHELXL-97.[41] The refined Flack parameter[42] was calculated using 9716 Friedel pairs and converged to a final value of 0.00(9), showing that the chosen configuration for the atomic model was the correct one. The structure showed disorder in several dichloromethane solvent molecules that were refined as isotropic. All the thiocoraline non-H atoms were allowed anisotropic thermal motion. The hydrogen atoms were included at calculated positions and were refined with a riding model and with Uiso. Calculations using PLATON[43] indicated that there were four symmetry equivalent voids of 35 Å^3 each, which were not big enough to contain additional solvent molecules. Thermal ellipsoid plots were obtained using the program ORTEP-3 for Windows.[44] All calculations were carried out using the WinGX package[45] of crystallographic programs. The supplementary crystallographic data for this article can be obtained free of charge from the Cambridge Crystallographic Data Centre via www.ccdc.cam.ac.uk/data_request/cif (id code 629608).

Purification of the DNA Restriction Fragment and Radiolabeling. The 117-bp DNA fragment was prepared by 3′-[^{32}P]-end labeling of the *Eco*RI-*Pvu*II double digest of the pBS plasmid using α-[^{32}P]-dATP (Amersham, 3000 Ci/mmol) and AMV reverse transcriptase (Roche). The labeled digestion products were separated on a 6% polyacrylamide gel under nondenaturing conditions in TBE buffer (89 mM Tris-borate, pH 8.3, 1 mM EDTA). After autoradiography, the requisite band of DNA was excised, crushed, and soaked in water overnight at 37 °C. This suspension was filtered through a Millipore 0.22 μm filter, and the DNA was precipitated with ethanol. Following washing with 70% ethanol and vacuum-drying of the precipitate, the labeled DNA was resuspended in 10 mM Tris, adjusted to pH 7.0, containing 10 mM NaCl.

DNase I Footprinting, Electrophoresis, and Autoradiography. Digestion of the samples (6 μL) of the labeled DNA fragment dissolved in 10 mM Tris buffer (pH 7.0) containing 10 mM NaCl was initiated by adding 2 μL of a DNase I (Sigma, L'Isle d'Abeau Chesnes, France) solution whose concentration had been adjusted to yield a final enzyme concentration of ∼0.01 units/mL in the reaction mixture. The extent of digestion was limited to <30% of the starting material to minimize the incidence of multiple cuts in any strand ("single-hit" kinetic conditions). Optimal enzyme dilutions were established in preliminary calibration experiments. After 3 min, the digestion was stopped by freeze-drying. Samples were lyophilized, washed once with 50 μL of water, lyophilized again, and then resuspended in 4 μL of an 80% formamide solution containing tracking dyes. Samples were heated at 90 °C for 4 min and chilled in ice for 4 min prior to electrophoresis. DNA cleavage products were resolved by polyacrylamide gel electrophoresis under denaturing conditions (0.3 mm thick, 8% acrylamide containing 8 M urea) capable of resolving DNA fragments differing in length by one nucleotide. Electrophoresis was continued until the bromophenol blue marker had run out of the gel (∼2.5 h at 60 W, 1600 V in TBE buffer, BRL sequencer model S2). Gels were soaked in 10% acetic acid for 15 min, transferred to Whatman 3MM paper, dried under vacuum at 80 °C, and subjected to autoradiography at −70 °C with an intensifying screen. Exposure times of the X-ray films (Fuji R-X) were adjusted according to the number of counts per lane loaded on each individual gel (usually 24 h). A Molecular Dynamics 425E PhosphorImager was used to collect data from storage screens exposed to the dried gels overnight at room temperature. Footprinting data are presented in the form $\ln(f_a) - \ln(f_c)$ representing the differential cleavage at each bond relative to that in the control (f_a is the fractional cleavage at any bond in the presence of the drug, and f_c is the fractional cleavage of the same bond in the control), as explained in detail before.[13] Logarithmic positive values indicate enhanced cleavage, whereas negative values indicate blockage.

Fluorescent Melting Experiments. Synthetic oligodeoxynucleotides with one strand 5′-end-labeled with the fluorophore 6-carboxyfluorescein (6-FAM, F) and the complementary strand 3′-end-labeled with the fluorescence quencher tetramethylrhodamine (TAMRA, Q) were synthesized by Bonsai Technologies Group S.A. (Avda. Valdelaparra 27, 28108 Alcobendas, Madrid, Spain) on either the 0.2 or 1 μmol scale and were purified by high-performance liquid chromatography as a single peak. Annealing

of each F oligonucleotide with its complementary Q oligonucleotide at a final duplex concentration of 0.1 μM in TAE buffer (0.08 M Tris-acetate, 2 mM EDTA, pH 7.5) was accomplished in a PTC-100 thermocycler (MJ Research, Inc. Waltham, MA) by first heating to 95 °C for 5 min and then gradually cooling to 20 °C at a rate of 1 °C min^{-1}. Correct annealing was confirmed because when the oligonucleotides form a double-stranded structure, F and Q are placed in proximity so that the fluorescence of F is quenched.

The melting reactions were carried out in 96-well plates loaded with the double-stranded preannealed oligonucleotides in a total volume of 20 μL of TAE buffer at a final concentration of 0.1 μM either in the absence or in the presence of the drug. Thiocoraline and echinomycin were dissolved in dimethyl sulfoxide and serially diluted in the same solvent to yield final concentrations from 10^{-5} to 10^{-8} M. The mixtures were incubated in all cases for 60 min at 37 °C before the melting assay was started in a 7500 Fast Real-Time PCR System (ABI Prism, Applied Biosystems) by increasing the temperature in small steps of 1 °C min^{-1} up to 95 °C. Upon heating, a temperature is reached at which the double strand melts so that groups F and Q are separated and the fluorescence increases. By recording the changes in fluorescence at 517 nm in the FAM channel obtained as a function of the temperature and calculating the midpoint of the transition (T_m), we have been able to estimate the increases in melting temperatures (ΔT_m) brought about by drug binding and the ligand concentration that produces half the maximal change in melting temperature (C_{50}). For the preliminary studies the following oligonucleotides (and their 3′-Q-labeled complementary strands) were used: 5′-F-d(CAATTAAATATAAC) and 5′-F-d(GCGCGGCGTCCGGGCC). These sequences were designed to provide nearly all of the possible subsequences of four bases formed by A and T or G and C, respectively, that could be recognized by the drug while at the same time minimizing the possibility of incorrect annealing. Custom oligonucleotides embedding a variety of central single or double steps were also designed to further delineate the binding preferences including the sites flanking the bisintercalation step. The sequences of all the fluorescently labeled oligonucleotides used are shown in Table 1. The raw data recovered from the instrument for each plate consisted of an array of FAM fluorescence values for each of the 96 wells at each temperature. A complete analysis was carried out using an in-house Visual Basic Application running on Microsoft Excel. A series of standardized operations were then applied automatically to the complete data array, including adaptive Gaussian-like smoothing, user-supervised upper and lower background correction, data normalization, and calculation of the midpoint of the transition (manuscript in preparation).

Cell Cultures. Cells were maintained at 37 °C and 5% CO_2 in Dulbecco's modified Eagle's medium (DMEM) supplemented with 10% fetal calf serum and 100 units/mL penicillin and streptomycin. All the tumor cell lines used in this study were obtained from the American Type Culture Collection (ATCC) unless otherwise indicated: DU-145 (brain metastatic site, ATCC HTB-81) and LNcaP (left supraclavicular lymph node metastatic site, ATCC CRL-1740), prostate carcinoma; IGROV,[46] ovary carcinoma; SK-BR-3 (pleural effusion, ATCC HTB-30), breast adenocarcinoma; SK-MEL-28 (ATCC HTB-72), melanoma; A-549 (ATCC CCL-185), lung carcinoma; K-562 (ATCC CCL-243), chronic myelogenous leukemia; PANC-1 (ATCC CRL-1469), pancreatic ductal carcinoma; HT-29 (ATCC HTB-38); LoVo (left supraclavicular region metastatic site, ATCC CCL-229); LoVo-Dox (a subclone of LoVo cells overexpressing the drug efflux pump MDR1/Pgp170);[47] and HeLa (ATCC CCL-2), cervix carcinoma.

Growth Inhibition Assay. A colorimetric assay using sulforhodamine B (SRB)[15] was adapted for quantitative measurement of cell growth and viability, as previously described.[48,49] Briefly, cells were seeded in 96-well microtiter plates and allowed to settle for 24 h in drug-free medium before treatment with vehicle alone or thiocoraline for 72 h. For quantification, cells were washed twice with phosphate buffered saline (PBS), fixed for 15 min in 1% glutaraldehyde solution, rinsed twice with PBS, stained in 0.4% SRB−1% acetic acid solution for 30 min, rinsed several times with 1% acetic acid solution, and air-dried. SRB was then extracted in 10 mM Trizma base solution, and the optical density was measured at 490 nm in a microplate spectrophotometer. Cytotoxicity was estimated applying the National Cancer Institute (NCI) algorithm.[50] If T_z is the number of control cells at time zero, C is the number of cells in control wells at 72 h, and T is the number of cells in the test wells at 72 h and if $T_z < T < C$ (no effect or growth inhibition), then cell survival is $100 \times ([T - T_z]/[C - T_z])$. If $T < T_z$ (net cell killing), then cell survival is $100 \times ([T - T_z]/T_z)$. Three dose response parameters were calculated for each experimental agent:[51] (i) GI_{50}, or compound concentration that produces 50% inhibition on cell growth compared to control cells; (ii) TGI, or compound concentration that produces total growth inhibition as compared to control cells; (iii) LC_{50}, or compound concentration that produces 50% net cell killing.

Building, Refinement, and Molecular Dynamics of the Thiocoraline−DNA Complexes. The models previously built for echinomycin[52] and 2QN[22] bound to DNA hexamers or decamers containing a central CpG step were used for modeling the 1:1 complexes of either thiocoraline or echinomycin with the symmetrical octanucleotides $[d(CTA\underline{CG}TAG)]_2$ and $[d(CAT\underline{CG}ATG)]_2$ and the nonsymmetrical octanucleotide d(CAA<u>CG</u>ATG)·d(CAT<u>CG</u>TTG) and also a 1:1 complex of thiocoraline with the d(CT<u>AC</u>CAAG)·d(CTTGGTAG) duplex. In all cases every base pair was in the Watson−Crick conformation. Appropriate modifications of base composition were introduced where necessary using standard geometries, and the X-ray crystal structure of thiocoraline (this work) was then optimally overlaid onto DNA-bound echinomycin or 2QN using the best-fit superimposition facility available in the computer graphics program PyMOL.[53]

The thiocoraline molecule was broken down into suitable fragments (Figure 1). The charge distribution for each of the nonstandard residues of thiocoraline (i.e., 3-hydroxyquinaldic acid, *N*,*S*-dimethyl-(*S*)-cysteine, and *N*-methyl-(*S*)-cysteine) was derived by fitting the quantum mechanically calculated (RHF 6-31G*//3-21G*)[54] molecular electrostatic potential (MEP) to a point charge model using the RESP methodology.[55] Appropriate bonded and nonbonded parameters consistent with the second-generation AMBER force field[56] (parm99) were assigned by analogy or through interpolation from those already present in the AMBER database (Supporting Information). The parameters for the thioester linkage between D-Cys and *N*,*S*-dimethyl-(*S*)-Cys residues were calculated to reproduce in the molecular mechanics force field using SPASMS[57] the torsional barrier calculated ab initio in Gaussian 98 (keyword SCAN)[54] by rotating the bond in steps of 15° (Supporting Information).

Each complex was then neutralized by addition of 14 sodium ions[58] that were placed in electrostatically favored positions and immersed in rectangular boxes each containing ∼2400 TIP3P water molecules[59] that extended 8 Å away from any solute atom. The cutoff distance for the nonbonded interactions was 9 Å, and periodic boundary conditions were applied. Electrostatic interactions were represented using the smooth particle mesh Ewald method with a grid spacing of ∼1 Å. Solvent molecules and counterions were relaxed by energy minimization and allowed to redistribute around the positionally restrained solute (25 kcal mol^{-1} $Å^{-2}$) during 50 ps of molecular dynamics (MD) at constant temperature (300 K) and pressure (1 atm) using the SANDER module in AMBER 8.[57] The coupling constants for the temperature and pressure baths were 1.0 and 0.2 ps, respectively. SHAKE[60] was applied to all bonds involving hydrogens, and an integration step of 2 fs was used throughout. The nonbonded pair list was updated every 10 steps. These initial harmonic restraints were then gradually reduced until their complete removal in a series of progressive energy minimizations, as recently described.[31] The resulting systems were heated again from 100 to 300 K during 20 ps and allowed to equilibrate for 1.0 ns of unrestrained MD before a production run of 2.0 ns, during which system coordinates were collected every 2 ps for further analysis.

Analysis of the Molecular Dynamics Trajectories and Electrostatic Energy Calculations. Three-dimensional structures and

trajectories were visually inspected using the computer graphics program PyMOL.[53] Interatomic distances and angles were monitored using the CARNAL module in AMBER. Finite difference solutions to the linearized Poisson−Boltzmann equation, as implemented in the DelPhi module (version 2.5) of Insight II (Accelrys), were used to calculate MEPs and electrostatic free energies. For MEP calculations on echinomycin and thiocoraline, cubic grids with a resolution of 1.0 Å were centered on each molecule, and the atomic charges were distributed onto the grid points. AMBER charges and radii were used. Solvent-accessible surfaces, calculated with a spherical probe with a radius of 1.4 Å, defined the solute boundaries, and a minimum separation of 10 Å was left between any solute atom and the borders of the box. The potentials at the grid points delimiting the box were calculated analytically by treating each charge atom as a Debye−Hückel sphere. The interior of both the DNA and the ligand was considered a low-dielectric medium ($\epsilon = 2$), whereas the surrounding solvent was treated as a high-dielectric medium ($\epsilon = 80$) with an ionic strength of 0.145 M. Intermolecular van der Waals energies for individual residues were calculated with the ANAL module, whereas the solvent-corrected residue-based electrostatic interaction energies were calculated with DelPhi, following the procedure described in detail elsewhere.[61,62]

All the calculations were performed on the SGI R10000 Power Challenge at Alcalá University Computer Center, on the SGI R14000 Origin 3800 at CIEMAT (Madrid), and locally on Dual Xenon 3.2 GHz Dell Precision 670-N workstations.

Acknowledgment. During the course of this work E.M. enjoyed a fellowship from Junta de Comunidades de Castilla-La Mancha, J.J.V. was supported by Grant MCYT-BQU2005-01060CTQ, and V.G.-H. was supported by Consejería de Educación de la Comunidad de Madrid and the European Social Fund (F.S.E.). We gratefully acknowledge support from the Ligue Nationale Contre le Cancer (Comité du Nord) and the Institut de Recherches sur le Cancer de Lille (IRCL) (to C.B.) and the Spanish CICYT (Grant SAF2003-7219-C02), PharmaMar (Colmenar Viejo, Madrid), and the National Foundation for Cancer Research (to F.G.). We thank the University of Alcalá Computing Centre and the CIEMAT (Madrid) for generous allowances of computer time on their SGI servers.

Supporting Information Available: Results from X-ray crystallographic analysis, AMBER PREP files for thiocoraline, ORTEP representations of the crystal structure, and figures showing the torsional barrier around the thioester bond and the drug−DNA electrostatic interaction energy decomposition. This material is available free of charge via the Internet at http://pubs.acs.org.

References

(1) Romero, F.; Espliego, F.; Baz, J. P.; de Quesada, T. G.; Grávalos, D.; de la Calle, F.; Fernández-Puentes, J. L. Thiocoraline, a new depsipeptide with antitumor activity produced by a marine *Micromonospora*. I. Taxonomy, fermentation, isolation, and biological activities. *J. Antibiot.* **1997**, *50*, 734−737.

(2) Pérez Baz, J.; Canedo, L. M.; Fernández-Puentes, J. L. Thiocoraline, a novel depsipeptide with antitumor activity produced by a marine *Micromonospora*. II. Physico-chemical properties and structure determination. *J. Antibiot.* **1997**, *50*, 738−741.

(3) Lombo, F.; Velasco, A.; Castro, A.; de la Calle, F.; Braña, A. F.; Sánchez-Puelles, J. M.; Méndez, C.; Salas, J. A. Deciphering the biosynthesis pathway of the antitumor thiocoraline from a marine actinomycete and its expression in two streptomyces species. *ChemBioChem* **2006**, *7*, 366−376.

(4) Boger, D. L.; Ichikawa, S.; Tse, W. C.; Hedrick, M. P.; Jin, Q. Total syntheses of thiocoraline and BE-22179 and assessment of their DNA binding and biological properties. *J. Am. Chem. Soc.* **2001**, *123*, 561−568.

(5) Erba, E.; Bergamaschi, D.; Ronzoni, S.; Taverna, S.; Bonfanti, M.; Catapano, C. V.; Faircloth, G.; Jimeno, J.; D'lncalci, M. Mode of action of thiocoraline, a natural marine compound with anti-tumour activity. *Br. J. Cancer* **1999**, *80*, 971−980.

(6) Waring, M. J. Echinomycin and Related Quinoxaline Antibiotics. In *Molecular Aspects of Anticancer Drug−DNA Interactions*; Neidle, S., Waring, M. J., Eds.; Macmillan & Co.: London, 1993; Vol. 1, pp 213−242.

(7) Waring, M. J.; Wakelin, L. P. G. Echinomycin: a bifunctional intercalating antibiotic. *Nature* **1974**, *252*, 653−657.

(8) Ughetto, G.; Wang, A. H.; Quigley, G. J.; van der Marel, G. A.; van Boom, J. H.; Rich, A. A comparison of the structure of echinomycin and triostin A complexed to a DNA fragment. *Nucleic Acids Res.* **1985**, *13*, 2305−2323.

(9) Boger, D. L.; Ichikawa, S. Total syntheses of thiocoraline and BE-22179: establishment of relative and absolute stereochemistry. *J. Am. Chem. Soc.* **2000**, *122*, 2956−2957.

(10) Boger, D. L.; Chen, J.-H. (−)-Sandramycin: total synthesis and preliminary DNA binding properties *J. Am. Chem. Soc.* **1993**, *115*, 11624−11625.

(11) Boger, D. L. U.S. Patent Application 20040072738, April, 15, 2004. URL: http://www.patentdebate.com/PATAPP/20040072738.

(12) Darby, R. A.; Sollogoub, M.; McKeen, C.; Brown, L.; Risitano, A.; Brown, N.; Barton, C.; Brown, T.; Fox, K. R. High throughput measurement of duplex, triplex and quadruplex melting curves using molecular beacons and a LightCycler. *Nucleic Acids Res.* **2002**, *30*, e39.

(13) Fox, K. R.; Gauvreau, D.; Goodwin, D. C.; Waring, M. J. Binding of quinoline analogues of echinomycin to deoxyribonucleic acid. Role of the chromophores. *Biochem. J.* **1980**, *191*, 729−742.

(14) Gauvreau, D.; Waring, M. J. Directed biosynthesis of novel derivatives of echinomycin by *Streptomyces echinatus*. I. Effect of exogenous analogues of quinoxaline-2-carboxylic acid on the fermentation. *Can. J. Microbiol.* **1984**, *30*, 439−450.

(15) Skehan, P.; Storeng, R.; Scudiero, D.; Monks, A.; McMahon, J.; Vistica, D.; Waren, J. T.; Bokesch, H.; Kenney, S.; Boyd, M. R. New colorimetric cytotoxicity assay for anticancer drug screening. *J. Natl. Cancer Inst.* **1990**, *82*, 1107−1112.

(16) Allen, F. H. The Cambridge Structural Database: a quarter of a million crystal structures and rising. *Acta Crystallogr.* **2002**, *B58*, 380−388.

(17) Sheldrick, G. M.; Heine, A.; Schmidt-Base, K.; Pohl, E.; Jones, P. G.; Paulus, E.; Waring, M. J. Structures of quinoxaline antibiotics. *Acta Crystallogr. B* **1995**, *51*, 987−999.

(18) Sheldrick, G. M.; Guy, J. J.; Kennard, O.; Rivera, V.; Waring, M. J. Crystal and molecular structure of the DNA-binding antitumour antibiotic triostin A. *J. Chem. Soc., Perkin Trans. 2* **1984**, *10*, 1601−1605.

(19) Hossain, M. B.; van der Helm, D.; Olsen, R. K.; Jones, P. G.; Sheldrick, G. M.; Egert, E.; Kennard, O.; Waring, M. J.; Viswamitra, M. A. Crystal and molecular structure of the quinoxaline antibiotic analog TANDEM (des-*N*-tetramethyltriostin A). *J. Am. Chem. Soc.* **1982**, *104*, 3401−3408.

(20) Searle, M. S.; Hall, J. G.; Wakelin, P. G. ^{1}H- and ^{13}C-n.m.r. studies of the antitumour antibiotic luzopeptin. Resonance assignments, conformation and flexibility in solution. *Biochem. J.* **1988**, *256*, 271−278.

(21) Low, C. M.; Fox, K. R.; Waring, M. J. DNA sequence selectivity of three biosynthetic analogues of the quinoxaline antibiotics. *Anti-Cancer Drug Des.* **1986**, *1*, 149−160.

(22) Bailly, C.; Echepare, S.; Gago, F.; Waring, M. J. Recognition elements that determine affinity and sequence-specific binding to DNA of 2QN, a biosynthetic bis-quinoline analogue of echinomycin. *Anti-Cancer Drug Des.* **1999**, *14*, 291−303.

(23) Bailly, C.; Waring, M. J. Comparison of different footprinting methodologies for detecting binding sites for a small ligand on DNA. *J. Biomol. Struct. Dyn.* **1995**, *12*, 869−898.

(24) Fletcher, M. C.; Fox, K. R. Dissociation kinetics of echinomycin from CpG binding sites in different sequence environments. *Biochemistry* **1996**, *35*, 1064−1075.

(25) Bailly, C.; Hamy, F.; Waring, M. J. Cooperativity in the binding of echinomycin to DNA fragments containing closely spaced CpG sites. *Biochemistry* **1996**, *35*, 1150−1161.

(26) Fox, K. R.; Marks, J. N.; Waterloh, K. Echinomycin binding to alternating AT. *Nucleic Acids Res.* **1991**, *19*, 6725−6730.

(27) Gago, F. Stacking interactions and intercalative DNA binding. *Methods* **1998**, *14*, 277−292.

(28) Marchand, C.; Bailly, C.; McLean, M.; Moroney, S. E.; Waring, M. J. The 2-amino group of guanine is absolutely required for specific binding of the anti-cancer antibiotic echinomycin to DNA. *Nucleic Acids Res.* **1992**, *20*, 5601−5606.

(29) Gilbert, D. E.; Feigon, J. The DNA sequence at echinomycin binding sites determines the structural changes induced by drug binding: NMR studies of echinomycin binding to $[d(ACGTACGT)]_2$ and $[d(TCGATCGA)]_2$. *Biochemistry* **1991**, *30*, 2483−2494.

(30) Cuesta-Seijo, J. A.; Sheldrick, G. M. Structures of complexes between echinomycin and duplex DNA. *Acta Crystallogr., Sect. D: Biol. Crystallogr*. **2005**, *61*, 442−448.
(31) Marco, E.; Negri, A.; Luque, F. J.; Gago, F. Role of stacking interactions in the binding sequence preferences of DNA bis-intercalators: insight from thermodynamic integration free energy simulations. *Nucleic Acids Res.* **2005**, *33*, 6214−6224.
(32) Gallego, J.; Ortiz, A. R.; Gago, F. A molecular dynamics study of the bis-intercalation complexes of echinomycin with $d(ACGT)_2$ and $d(TCGA)_2$: rationale for sequence-specific Hoogsteen base-pairing. *J. Med. Chem*. **1993**, *36*, 1548−1561.
(33) Kong, D.; Park, E. J.; Stephen, A. G.; Calvani, M.; Cardellina, J. H.; Monks, A.; Fisher, R. J.; Shoemaker, R. H.; Melillo, G. Echinomycin, a small-molecule inhibitor of hypoxia-inducible factor-1 DNA-binding activity. *Cancer Res.* **2005**, *65*, 9047−9055.
(34) Semenza, G. L. Targeting HIF-1 for cancer therapy. *Nat. Rev. Cancer* **2003**, *3*, 721−732.
(35) Burke, T. W.; Kadonaga, J. T. The downstream core promoter element, DPE, is conserved from *Drosophila* to humans and is recognized by TAFII60 of *Drosophila*. *Genes Dev.* **1997**, *11*, 3020−3031.
(36) Kadonaga, J. T. The DPE, a core promoter element for transcription by RNA polymerase II. *Exp. Mol. Med*. **2002**, *34*, 259−264.
(37) Lavesa, M.; Fox, K. R. Preferred binding sites for [*N*-$MeCys^3$, *N*-$MeCys^7$]TANDEM determined using a universal footprinting substrate. *Anal. Biochem.* **2001**, *293*, 246−250.
(38) James, P. L.; Merkina, E. E.; Khalaf, A. I.; Suckling, C. J.; Waigh, R. D.; Brown, T.; Fox, K. R. DNA sequence recognition by an isopropyl substituted thiazole polyamide. *Nucleic Acids Res.* **2004**, *32*, 3410−3417.
(39) North, A. C. T.; Phillips, D. C.; Mathews, F. S. A semi-empirical method of absorption correction. *Acta Crystallogr., Sect. A* **1968**, *24*, 351−359.
(40) Burla, M. C.; Caliandro, R.; Camalli, M.; Carrozzini, B.; Cascarano, G. L.; De Caro, L.; Giacovazzo, C.; Polidori, G.; Spagna, R. Sir2004: an improved tool for crystal structure determination and refinement. *J. Appl. Crystallogr*. **2005**, *38*, 381−388.
(41) Sheldrick, G. M. *SHELXL-97, a Program for Crystal Structure Refinement*, release 97-2; University of Göttingen: Göttingen, Germany.
(42) Flack, H. D. On enantiomorph-polarity estimation. *Acta Crystallogr*. **1983**, *A39*, 876−881.
(43) Spek, A. L. PLATON, an integrated tool for the analysis of the results of a single-crystal structure determination. *Acta Crystallogr*. **1990**, *A46*, C34.
(44) Farrugia, L. J. ORTEP-3 for Windows, a version of ORTEP-III with a graphical user interface (GUI). *J. Appl. Crystallogr*. **1997**, *30*, 565−565.
(45) Farrugia, L. J. WinGX suite for small-molecule single-crystal crystallography. *J. Appl. Crystallogr*. **1999**, *32*, 837−838.
(46) Benard, J.; Da Silva, J.; De Blois, M. C.; Boyer, P.; Duvillard, P.; Chiric, E.; Riou, G. Characterization of a human ovarian adenocarcinoma line, IGROV1, in tissue culture and in nude mice. *Cancer Res.* **1985**, *45*, 4970−4979.
(47) Grandi, M.; Geroni, C.; Giuliani, F. C. Isolation and characterization of a human colon adenocarcinoma cell line resistant to doxorubicin. *Br. J. Cancer* **1986**, *54*, 515−518.
(48) Faircloth, G. T.; Stewart, D.; Clement, J. J. A simple screening procedure for the quantitative measurement of cytotoxicity assay. *J. Tissue Cult. Methods* **1988**, *11*, 201−205.
(49) Vichai, V.; Kirtikara, K. Sulforhodamine B colorimetric assay for cytotoxicity screening. *Nat. Protoc.* **2006**, *1*, 1112−1116.
(50) Boyd, M. R.; Paull, K. D. Some practical considerations and applications of the National Cancer Institute in vitro anticancer drug discovery screen. *Drug Dev. Res*. **1995**, *34*, 91−109.
(51) Monks, A.; Scudiero, D.; Skehan, P.; Shoemaker, R.; Paull, K.; Vistica, D.; Hose, C.; Langley, J.; Cronise, P.; Vaigro-Wolff, A.; Gray-Goodrich, M.; Campbell, H.; Mayo, J.; Boyd, M. Feasibility of a high-flux anticancer drug screen using a diverse panel of cultured human tumor cell lines. *J. Natl. Cancer Inst.* **1991**, *83*, 757−766.
(52) Gallego, J.; Luque, F. J.; Orozco, M.; Burgos, C.; Alvarez-Builla, J.; Rodrigo, M. M.; Gago, F. DNA sequence-specific reading by echinomycin: role of hydrogen bonding and stacking interactions. *J. Med. Chem.* **1994**, *37*, 1602−1609.
(53) De Lano, W. DeLano Scientific LLC. URL: http://www.pymol.org/.
(54) Frisch, M. J.; Trucks, G. W.; Schlegel, H. B.; Scuseria, G. E.; Robb, M. A.; Cheeseman, J. R.; Zakrzewski, V. G.; Montgomery, J. A., Jr.; Stratmann, R. E.; Burant, J. C.; Dapprich, S.; Millam, J. M.; Daniels, A. D.; Kudin, K. N.; Strain, M. C.; Farkas, O.; Tomasi, J.; Barone, V.; Cossi, M.; Cammi, R.; Mennucci, B.; Pomelli, C.; Adamo, C.; Clifford, S.; Ochterski, J.; Petersson, G. A.; Ayala, P. Y.; Cui, Q.; Morokuma, K.; Malick, D. K.; Rabuck, A. D.; Raghavachari, K.; Foresman, J. B.; Cioslowski, J.; Ortiz, J. V.; Stefanov, B. B.; Liu, G.; Liashenko, A.; Piskorz, P.; Komaromi, I.; Gomperts, R.; Martin, R. L.; Fox, D. J.; Keith, T.; Al-Laham, M. A.; Peng, C. Y.; Nanayakkara, A.; Gonzalez, C.; Challacombe, M.; Gill, P. M. W.; Johnson, B. G.; Chen, W.; Wong, M. W.; Andres, J. L.; Head-Gordon, M.; Replogle, E. S.; Pople, J. A. *Gaussian 98*, revision A.11.2; Gaussian, Inc.: Pittsburgh, PA, 2001.
(55) Bayly, C. I.; Cieplak, P.; Cornell, W. D.; Kollman, P. A. A well-behaved electrostatic potential based method using charge restraints for deriving atomic charges: the RESP model. *J. Phys. Chem*. **1993**, *97*, 10269−10280.
(56) Cornell, W. D.; Cieplak, P.; Bayly, C. I.; Gould, I. R.; Merz, K. M.; Ferguson, D. M.; Spellmeyer, D. C.; Fox, T.; Caldwell, J. W.; Kollman, P. A. A second generation force field for the simulation of proteins, nucleic acids, and organic molecules. *J. Am. Chem. Soc*. **1995**, *117*, 5179−5197.
(57) URL: http://amber.scripps.edu/doc8/.
(58) Åqvist, J. Ion−water interaction potentials derived from free energy perturbation simulations. *J. Phys. Chem*. **1990**, *94*, 8021−8024.
(59) Jorgensen, W. L.; Chandrasekhar, J.; Madura, J. D. Comparison of simple potential functions for simulating liquid water. *J. Chem. Phys.* **1983**, *79*, 926−935.
(60) Ryckaert, J. P.; Ciccoti, G.; Berendsen, H. J. C. Numerical integration of the Cartesian equations of motion of a system with constraints: molecular dynamics of *n*-alkanes. *J. Comput. Phys*. **1977**, *23*, 327−341.
(61) Gallego, J.; Ortiz, A. R.; de Pascual-Teresa, B.; Gago, F. Structure−affinity relationships for the binding of actinomycin D to DNA. *J. Comput.-Aided Mol. Des.* **1997**, *11*, 114−128.
(62) Pérez, C.; Ortiz, A. R.; Pastor, M.; Gago, F. Comparative binding energy analysis of HIV-1 protease inhibitors: incorporation of solvent effects and validation as a powerful tool in receptor-based drug design. *J. Med. Chem*. **1998**, *41*, 836−852.

JM070381S